Micron 145 (2021) 103063

Contents lists available at ScienceDirect

Micron

journal homepage: www.elsevier.com/locate/micron

Functional analyses of chitinolytic enzymes in the formation of calcite prisms in *Pinctada fucata*

Hiroyuki Kintsu [a,b], Alberto Pérez-Huerta [c], Shigeru Ohtsuka [d], Taiga Okumura [e], Shinsuke Ifuku [f], Koji Nagata [a], Toshihiro Kogure [e], Michio Suzuki [a,*]

[a] Department of Applied Biological Chemistry, Graduate School of Agricultural and Life Sciences, The University of Tokyo, Tokyo, 113-8657, Japan
[b] National Institute for Environmental Studies, Ibaraki, 305-8506, Japan
[c] Department of Geological Sciences, The University of Alabama, Tuscaloosa, AL, 35487, USA
[d] Institute of Engineering Innovation, The University of Tokyo, Tokyo, 113-8656, Japan
[e] Department of Earth and Planetary Science, Graduate School of Science, The University of Tokyo, Tokyo, Japan
[f] Department of Chemistry and Biotechnology, Graduate School of Engineering, The University of Tottori, Tottori, 680-8552, Japan

ARTICLE INFO

Keywords:
Biomineralization
Calcite
Chitin
Chitinolytic enzymes
Pinctada fucata
Prismatic layer

ABSTRACT

The mollusk shells present distinctive microstructures that are formed by small amounts of organic matrices controlling the crystal growth of calcium carbonate. The shell of *Pinctada fucata* has the prismatic layer consisting of prisms of single calcite crystals and the nacreous layer consisting of aragonite tablets. The calcite crystal of prisms contains small angle grain boundaries caused by a dense intracrystalline organic matrix network to improve mechanical strength. Previously, we identified chitin and chitinolytic enzymes as components of this intracrystalline organic matrix. In this study, to reveal the function of those organic matrices in calcium carbonate crystallization, calcites synthesized in chitin gel with or without chitinolytic enzymes were analyzed by using transmission electron microscope (TEM) and atom probe tomography (APT), showing ion clusters derived from chitin inside of a calcite and small angle grain boundaries at optimal chitinolytic concentration. Furthermore, we performed the experiment in which chitinase inhibitor was injected into a living *P. fucata*. Nanoindentation and electron back scattered diffraction (EBSD) show that mechanical properties and crystal orientation were changed. These results suggested that chitinolytic enzymes work cooperatively with chitin to regulate the crystal growth and mechanical properties of the prismatic layer.

1. Introduction

Molluscan shells consist of more than 90 % calcium carbonate and small amounts of organic matrices, which interact with calcium carbonate and regulate its crystallization. The organic matrices may be classified into three groups: insoluble organic matrices (IOMs) such as chitin (Furuhashi et al., 2009b, 2009a; Levi-Kalisman et al., 2001; Suzuki et al., 2007; Weiner et al., 1984; Weiner and Traub, 1980), soluble organic matrices (SOMs) binding IOMs with a domain that can interact with IOMs (Marie et al., 2011; Montagnani et al., 2011; Suzuki et al., 2011, 2009), and SOMs that exist freely (Miyamoto et al., 1996; Sudo et al., 1997; Weiner and Hood, 1975). IOMs generally provide the scaffold for crystallization, and SOMs contain acidic domains such as Asp-rich regions, which control the crystal polymorph, morphology, and growth. Such organic-inorganic interactions can generate a fine microstructure. However, most of the detailed structures and functions of these organic molecules are still unknown.

Pinctada fucata, a bivalve used for pearl cultivation, has a microstructure composed of prismatic and nacreous layers in its shell. The prismatic layer exists on the outer layer of shells, and is comprised of calcite prisms surrounded by an organic framework, which appears as a honeycomb structure (Checa et al., 2005; Nakahara and Bevelander, 1971; Suzuki et al., 2013). The radius and length of one calcite prism are approximately 20−40 μm and 100−150 μm, respectively. Previous studies have reported that the calcite prism of *P. fucata* exhibits unique characteristics. The calcite prism of *P. fucata* is not a complete single

* Corresponding author.
E-mail addresses: kintsu.hiroyuki@nies.go.jp (H. Kintsu), aphuerta@ua.edu (A. Pérez-Huerta), ohtsuka@sogo.t.u-tokyo.ac.jp (S. Ohtsuka), okumura@eps.s.u-tokyo.ac.jp (T. Okumura), sifuku@chem.tottori-u.ac.jp (S. Ifuku), aknagata@mail.ecc.u-tokyo.ac.jp (K. Nagata), kogure@eps.s.u-tokyo.ac.jp (T. Kogure), amichiwo@mail.ecc.u-tokyo.ac.jp (M. Suzuki).

https://doi.org/10.1016/j.micron.2021.103063
Received 16 February 2021; Received in revised form 25 March 2021; Accepted 26 March 2021
Available online 7 April 2021

crystal, but contains small angle grain boundaries, which are slight crystal misorientations (Gilbert et al., 2011; Okumura et al., 2010). This small crystal defects may improve the strength and toughness of the prismatic layer (Olson et al., 2013). Besides, organic matrices are localized in a network, along small angle grain boundaries, indicating that the organic networks might contribute to the formation of small angle grain boundaries (Okumura et al., 2012). Although it is difficult to artificially mimic the superior microstructure of calcite prisms, *P. fucata* easily produces these fine structures under normal temperature and pressure using organic matrices.

Organic molecules are soft, flexible and fracture resistant. On the other hand, inorganic minerals are hard and brittle. Organic-inorganic interaction induces the nano-size crystals, mesoscopic microstructure, regulated density of defects, uniformed crystal orientation and special chemical composition with trace elements. Organic-inorganic complex in biominerals combine the best of these properties and minimize the weaknesses as strong and tough materials. (Gao et al., 2003; Gilbert et al., 2005; Jackson et al., 1988; Kamat et al., 2000; Nudelman and Sommerdijk, 2012).

In the previous study, we researched the components of the organic networks and their function in the formation of small angle grain boundaries (Kintsu et al., 2017). From organic networks, chitin was identified as the primary component. In addition, the chitinolytic enzymes that degrade chitin were also identified from the proteins that formed a complex with chitin. When calcium carbonate was crystallized in chitin gel treated with chitinolytic enzymes to imitate the condition during the calcite prism formation, the shape of a synthesized calcite in the chitin gel was gradually changed into the round shape and the lattice distortion of the synthesized calcite increased, depending on the concentration of chitinolytic enzymes, whereas a typical rhombohedral calcite was observed in the chitin gel without treatment of chitinolytic enzymes.

This finding suggested that chitin and chitinolytic enzymes might work cooperatively to induce small angle grain boundaries of calcite. When allosamidin, a chitinase inhibitor, was injected into a living *P. fucata* to examine the function of chitinase during the formation of the prismatic layer, the abnormal structure of prisms was observed, indicating chitinase is necessary for the prism formation in *P. fucata*. The cross section of this prismatic layer prepared by focused ion beam (FIB) was observed by transmission electron microscope (TEM). TEM observations revealed that the thickness of chitin fiber after treatment of allosamidin became thicker than that of chitin fiber before the treatment. These results enabled us to propose that chitin which becomes thinner fibers by chitinolytic enzymes degrading may induce crystal defects.

In this study, we performed further analyses of the respective calcites which we synthesized *in vitro* and the prismatic layer of the chitinase-inhibited individuals *in vivo*. In the experiment focusing on the synthesized calcite, we investigated how chitin is changed by chitinolytic enzymes by TEM and atom probe tomography (APT). On the other hand, we prepared the prismatic layer inhibited by a chitinase inhibitor *in vivo*. We analyzed the crystal orientation of the prismatic layer by electron back scatted diffraction (EBSD) image and measured the hardness and elastic modulus of the prismatic layer by nano indentation. These experiments would provide us with the evidence that *P. fucata* utilizes chitinolytic enzymes to produce the unique crystal structure.

2. Material and methods

2.1. Preparation of living P. fucata

The Japanese pearl oyster P. fucata that is Mollusca Bivalvia Pterioida Pteriidae *Pincatada fucata* was cultured at Ago Bay by Fisheries Research Division, Mie Prefectural Science and Technology Promotion Center in Japan. Cultivation was according to the previous method (Kintsu et al., 2017). The shell structures and tissues of *P. fucata* were shown in Fig. S1.

2.2. Synthesis of calcium carbonate in the chitin hydrogel

Chitin hydrogel was prepared according to the previous method (Tamura et al., 2006). The prepared chitin hydrogel was treated with Yatalase (an enzyme complex containing chitinase and chitobiase activities from *Corynebacterium* sp. OZ-21; TaKaRa) as chitinolytic enzyme. Yatalase was added to this chitin hydrogel in various concentrations (0, 0.12, 1.2 mg/mL) and stirred for 24 h. After reaction, chitin hydrogel was filtered and washed with 10 mM calcium chloride to remove Yatalase. The washed chitin hydrogel was spread on a plate (33.5 mm x 33.5 mm). This plate was put into desiccator filled with the gas of 5 g of ammonium carbonate (Kanto Chemical), followed by the calcium carbonate crystallization in the chitin hydrogel for 24 h. Chitin hydrogel was dissolved with 50 % sodium hypochlorite to collect the calcium carbonate crystals.

2.3. Calcium carbonate crystallization using chitin nanofiber

1.1 % (w/v) chitin nanofiber in 0.5 % acetic acid solution was prepared (Ifuku et al., 2010). The chitin nanofiber solution was neutralization with 1 M NaOH. 10 mM calcium chlorite solution was added to the chitin nanofiber solution. Calcium carbonate was then crystallized in the chitin nanofiber solution using the same method described above. The formed calcium carbonate crystals were observed with SEM and the cross-sections prepared by FIB were observed by TEM.

2.4. TEM observations of the calcium carbonate crystals

The calcium carbonate crystals synthesized in the chitin hydrogel were washed with distilled water to remove the sodium hypochlorite. The inside of these calcium carbonate crystals was also observed by TEM to investigate the inside detailed microstructure. Electron-transparent thin specimens for TEM observation were prepared using a focused ion beam (FIB) (FB 2100, Hitachi). The samples were locally coated with tungsten and trimmed using Ga ion beam and thinned down to a final thickness of 200 nm. These electron-transparent specimens were observed with a JEM-2010UHR TEM (JEOL) operated at 200 kV. The intracrystalline organic matrices were imaged by Fresnel contrast, not focusing on the organic matrices.

2.5. Atom probe tomography

The method of ATP analysis was performed according to previous study (Pérez-Huerta et al., 2016). Briefly, the tip specimens of the synthesized calcium carbonate crystals were prepared with a radius of about 50 nm by using FIB. These specimens were ionized with the local electrode (LEAP 3000 XSi) of The University of Alabama. Parameters were following; laser pulse energy = 150 and 1300 pJ, detection rate = 2%, base temperature =50 K. Three dimensional reconstructions from data of ion distributions were performed using the CAMECA IVAS software platform (details in (Pérez-Huerta et al., 2019)).

2.6. Cultivation of P. fucata

Three individuals of *P. fucata* (the age is about one year) were selected for each condition of allosamidin injection, PBS injection and no injection, respectively. 500 mL of allosamidin solution (2 mg/mL allosamidin in PBS) was injected into the adductor muscle of *P. fucata* every three days for a month. The same volume of PBS solution was also injected into the adductor of another three individuals as a negative control experiment. The injected individuals were cultured in seawater at 20 °C. After cultivation, the mantle tissue and shells of each individual was collected. The mantle tissues were homogenized in the extract buffer (50 mM HEPES-KOH (pH 7.8)/420 mM KCl/0.1 mM EDTA/5 mM

MCl2/20 % glycerol), and the supernatant of protein extraction was extracted. The protein extraction was concentrated and desalted by ultrafiltration tube (M.W. 10,000 cut off). Each protein extraction was applied to chitinase activity measurement. 50 mL of protein extraction (protein concentration is 125 mg/mL in citrate-phosphate buffer (pH 7.5)) was mixed with 30 mL of citrate-phosphate buffer. And then, 20 mL of 50 mM 4-methylumbelliferyl-*N,N',N''*-triacetyl chitotrioside [4MU-$(GlcNAc)_3$] dissolved in *N,N'*-dimethylformamide was added as a substrate and incubated at 37 °C for 15 min for the enzyme reaction. 1 mL of 1 M glycine solution (pH 10.6) was added to stop the reaction, and the fluorescence of this solution as chitinase activity was measured at excitation of 360 nm and emission of 450 nm using fluorescent photometer.

2.7. EBSD micrography of the prismatic layer

Before EBSD analysis, samples of the prismatic layer were embedded in epoxy (Buehler) and cut with ISOMET (Buehler) to expose the vertical cross-section of the prismatic layer. The surface of specimen was polished with decreasing silicon carbide powder (32, 13 and 8 μm), subsequently with diamond suspension (6 μm), and finally with colloidal silica (0.06 μm). Crystallographic information including crystal phase and grain orientation on the surfaces was analyzed by a field emission scanning electron microscope (FE-SEM, JSM-7000 F, JEOL Ltd.) equipped with electron back scattered diff ;raction. Accelerating voltage is 20 kV and step size is 0.5 μm.

2.8. Nanoindentation

Similar to the preparation for EBSD, samples of the prismatic layer were firstly embedded in epoxy (Buehler) and cut with ISOMET (Buehler) to expose the surface {001} planes of the prismatic layer, subsequently polished with decreasing silicon carbide powder, diamond suspension and colloidal silica. The specimens were fixed on the glass substrate with adhesive to measure the hardness using DUH-211 (Shimadzu) equipped with triangular pyramidal indenter tip. For each indent, a load of 100 mN was applied with loading rate and unloading rate of 0.474 mN/s to the surface {001} planes. A total of 6–8 indentations were conducted at each sample. The hardness and reduced elastic modulus were calculated according to Oliver-Pharr method (Oliver and Pharr, 1992). After the measurement, the impressions were observed using SEM.

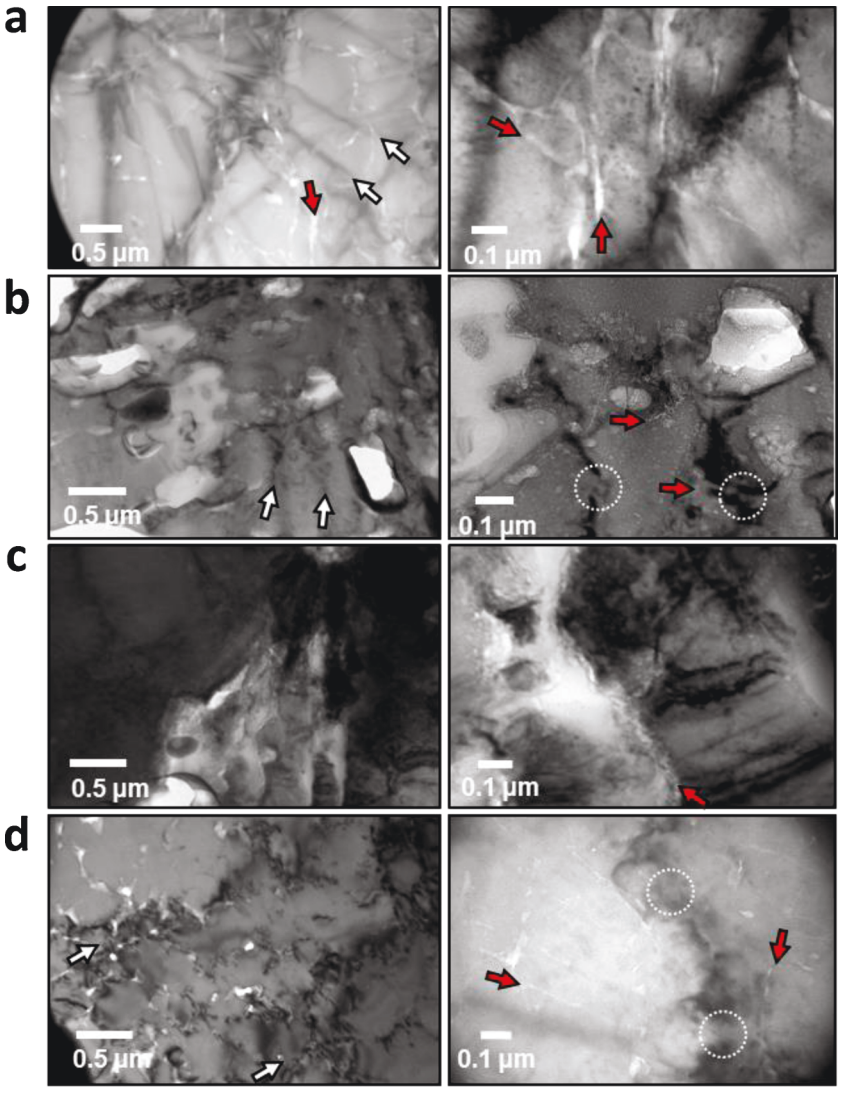

Fig. 1. TEM images of a cross section of the synthesized calcite crystals. a-c, the calcite crystal synthesized in chitin gel treated with chitinolytic enzymes at different concentration. a, 0 mg/mL; b, 0.12 mg/mL; and c, 1.2 mg/mL chitinolytic enzymes. d, calcite crystal synthesized in chitin nanofiber solution. Low magnification (left row) and high magnification (right row). White arrows denote interference fringes of equal inclination and red arrows denote voids of Fresnel contrasts indicating chitin fibers. White circles show that interference fringes of equal inclination become disordered lines suggesting that small angle grain boundaries occurred.

3. Results and discussion

3.1. Transmission electron microscope (TEM) observations of calcite crystals synthesized in chitin gels

Calcite crystals was synthesized in chitin gel with yatalase, a commercially available chitinolytic enzyme, at different concentration (0, 0.12 and 1.2 mg/mL) (Fig. S2). We also prepared calcite crystals synthesized in chitin nanofiber solution which is made by chemical and physical treatment and has uniformed thickness, because we predicted the thickness of chitin was important for the formation of crystal defects. Each calcite crystal was shaped into thin cross-section with focused ion beam (FIB) for transmission electron microscope (TEM) analysis. TEM bright field images of the cross-sections revealed that the calcite crystal formed in the chitin gel without yatalase treatment (0 mg/mL) contained many thick chitin fibers with a bright contrast indicated by red arrows in Fig. 1a. The bright contrast means the void of organic molecules inside the calcite crystal. The contrast of typical bend contour (interference fringe of equal inclination) which was observed in the single crystal indicated by white arrows in Fig. 1a was distributed in whole area, indicating that chitin gel without chitinolytic enzyme treatment did not affect the formation of crystal defects in calcite crystals. In addition, selected area electron diffraction (SAED) patterns reflected that the calcite crystals synthesized in these conditions were single crystals (Fig. S3a).

By contrast, following 0.12 mg/mL chitinolytic enzyme treatment (Fig. 1b), slightly disordered interference fringes were partially observed around the small spherical Fresnel contrasts indicated by red arrows. The small spherical Fresnel contrasts mean the localization of thin organic molecules (Okumura et al., 2012, 2010). The thin organic molecules might be a degraded chitin fiber by chitinolytic enzymes. If the sample was a perfect single crystal, equal inclination interference fringes would have shown clear straight lines. The disordered lines of interference fringes contrast showed that the small misorientations were generated. In Fig. 1b, interference fringes of equal inclination around the area of white circles were interrupted by lattice distortions generated by thin chitin fibers indicated by red arrows. These observations suggested that the positions of partial interrupted interference fringes corresponded to that of chitin fibers. SAED pattern (Fig. S3b) showed that the crystal orientation in whole area in Fig. 1b was almost uniformed, suggesting that the misorientation of crystal might be small. Thus, thin chitin fiber might induce the small angle grain boundaries in calcium carbonate crystals.

At 1.2 mg/mL chitinolytic enzyme treatment, thin chitin fibers were embedded with calcium carbonate. In Fig. 1c, the Fresnel contrasts means the position of thin chitin fibers indicated by red arrows. The interference fringes of equal inclination were completely stopped by the thin chitin fibers suggesting that the thin chitin fibers treated by 1.2 mg/mL yatalase made the perfect grain boundaries. The SAED pattern from the whole area in Fig. 1c showed the ring pattern (Fig. S3c), which means the calcite crystal containing grain boundaries was polycrystal. Since high concentration of yatalase decreased the thickness of chitin fiber, thinner chitin fiber might become the grain boundary.

Finally, we used the chitin nanofiber prepared by the physical treatments. In the chitin nanofiber solution, the interference fringes indicated by white arrows were disordered throughout the entire area (Fig. 1d). In the high magnification image, there were many Fresnel contrasts indicated by red arrows showing the distributions of chitin nanofibers. SAED pattern (Fig. S3d) showed that the crystal orientation in whole area in Fig. 1d was almost uniformed, suggesting that the misorientation of crystal might be small. This result was really similar to that of 0.12 mg/mL chitinolytic enzyme treatment. The chitin nanofibers interrupted the lines of interference fringes, suggesting that the small angle grain boundaries were generated around the areas of white circles in Fig. 1d

Based on these observations, TEM observations also supported the possibility that lattice distortion increased as the chitin fibers were degraded by chitinolytic enzymes, because the increasing surface areas of the chitin fibers strengthened the interactions between calcium carbonate and the chitin fiber. This strong interaction may have allowed chitin fibers to attach to the crystal growth front and inhibit growth of the crystal face in a random manner to induce a rounded shape.

3.2. Atom probe tomography (APT) of calcite crystals synthesized in chitin gels

Atom probe tomography (APT) is a useful technique to determine the three-dimensional (3D) distribution of atoms or ions in the materials (Gordon et al., 2012; Pérez-Huerta et al., 2016; Valley et al., 2014). In APT analysis, the specimen shaped into a needle-like tip with a radius of 50–100 nm by a focused ion beam was ionized by field evaporation to detect atoms of ions with 2D ion distributions, followed by a 3D reconstruction. In Fig. 2, the 3D reconstruction images show that ion clusters of COH^+ (yellow) and COH_2^+ (pink) derived from chitin are detected within calcium carbonate ions (red). Fragments of chitin were partially detected in calcium carbonate at a concentration of 0 mg/mL (Fig. 2a). Most of signals were localized in the edge of sample. These signals might be due to the artifact from the sample preparation. On the other hand, there were few signals inside the calcium carbonate. These results suggested that no treatment of chitinolytic enzymes made no distribution of chitin signals inside the calcium carbonate.

On the other hand, the yellow and pink signals of chitin increased and were distributed in wide area within calcium carbonate at higher concentrations (0.12 and 1.2 mg/mL) of chitinolytic enzymes (Fig. 2b, c). The continuous chitin signals were homogeneous. Almost all chitin signals appeared inside the calcite crystal. At 1.2 mg/mL chitinolytic enzyme treatment, the amounts of yellow and pink signals significantly increased (Fig. 2c). From these observations, these chitin signals might be derived from both chitin oligomers and chitin nanofibers degraded by chitinolytic enzymes. These APT results support the hypothesis that chitin without the treatment of chitinolytic enzymes could not give any molecules inside the calcite crystal, while high concentration of chitinolytic enzymes produced the small fragments of chitin and gave the impurities to the calcite lattice at the atomic level.

In case of the artificial chitin nanofiber produced by physical procedure, high density signals derived from chitin were detected (Fig. 2d). This result suggested that the chitin nanofibers were distributed homogeneously in calcite crystals and showed the high amounts of signals. This observation also supported the evidence that thin chitin fiber (oligomer or nanofiber) interacts with calcium carbonate inside the crystal.

3.3. Electron backscatter diffraction (EBSD) analyses of calcite prisms treated by chitinase inhibitor in vivo

As previously mentioned, we showed that chitinolytic enzymes may play important roles in formation of the *P. fucata* prismatic layer. To show the importance of chitinolytic enzymes on the formation of the prismatic layer, allosamidin, an inhibitor of GH18 chitinase (Sakuda et al., 1987), was injected into a living *P. fucata* every 3 days for a month. *P. fucata* was grown in natural sea water. Measurement of chitinase activity from mantle extracts showed that allosamidin suppressed activity for 1 month, indicating that the shell was formed under conditions of low chitinase activity (Fig. S4). If our hypothesis that chitinolytic enzymes degrade chitin and affect crystal growth was correct, the prism should be affected by inhibition of activity. Fig. 3 and Fig. S5 showed EBSD mapping of the surface and longitudinal cross-section of prismatic layers along the *c* axis, and line profiles of one prism. We chose the position of growth front in the prismatic layer to see the effect of inhibitor on the prism formation. In the normal prismatic layer without inhibitor, crystal orientation on the surface of calcite prisms were almost uniformed (Fig. S5a). The strong red color of mapping image on the

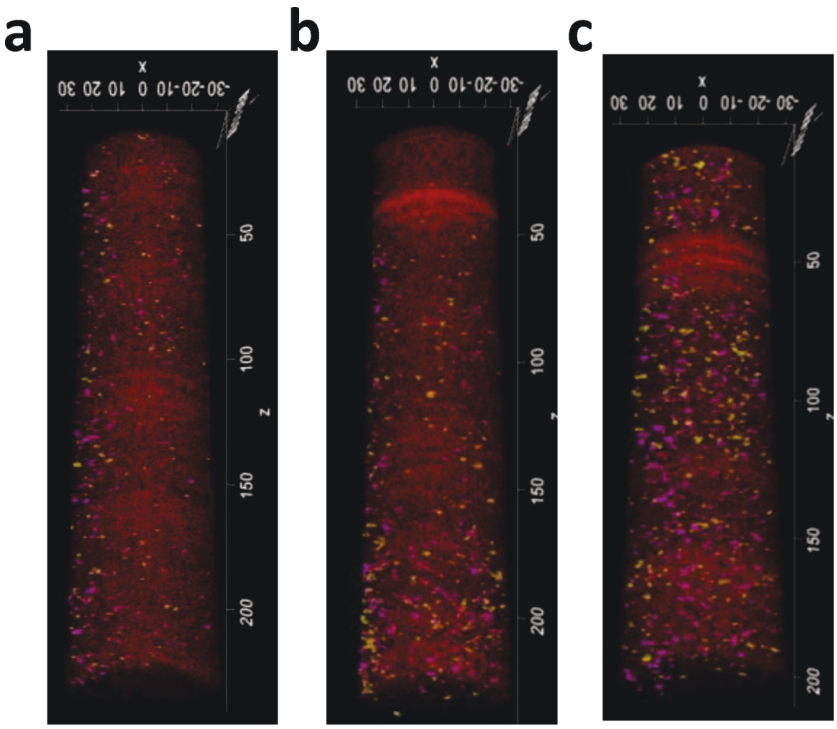

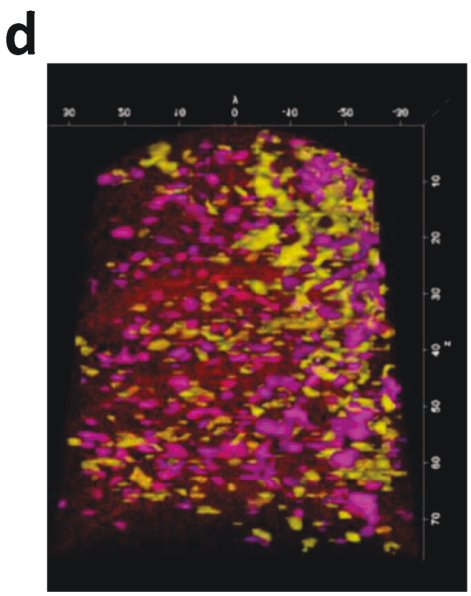

Fig. 2. Distribution of ions of the synthesizes calcite crystals using APT. Distribution images of ions from a direction parallel to a longitudinal tip shaped into from the synthesized calcite crystals using APT. a-c, the calcite crystal synthesized in chitin gel treated with chitinolytic enzymes at different concentration. a, 0 mg/mL; b, 0.12 mg/mL; and c, 1.2 mg/mL chitinolytic enzymes. d, calcite crystal synthesized in chitin nanofiber solution. Colors denote ion species; Ca^{2+} in red, COH^{+} in yellow and COH^{2+} in pink. COH^{+} and COH^{2+} are derived from chitin molecule.

surface area reflected that the *c* axis of calcite was almost perpendicular to the shell surface. Although the rotated *c* axis of calcite was observed in the part of small areas, this rotation of *c* axis in the prismatic layer was reported in the previous report (Dauphin et al., 2019). We also prepared the cross-section of prisms. The color of one prism was found to be uniform from mapping the image and angle spread of one prism measured from the line profile within 3 degrees; there was minimal crystal misorientation within one prism (Fig. 3a). However, in the prismatic layer treated with inhibitor, color image of the surface slightly changed. The orientations of *c* axis were not uniformed in various prisms (Fig. S5b). Furthermore, in the cross-section, the crystal orientation of one prism was found to be gradually changed, with the mapping image and angle spread of one prism approximately 10 degrees (Fig. 3b). The reason for the increase of angle spread was likely due to intracrystalline chitin thickening from inhibiting chitin degradation. We previously reported that thicker chitin fibers inside the calcite prism treated with allosamidin compared with those of normal calcite prism were observed using TEM (Kintsu et al., 2017). Chitin fibers that increased in thickness may have contributed to crystal misorientation.

3.4. Nanoindentation of calcite prisms treated by a chitinase inhibitor in vivo

A previous study reported that a biotic calcite crystal with slight crystal distortion was stronger than an abiotic calcite crystal without crystal distortion because the abiotic calcite is easily cracked under high

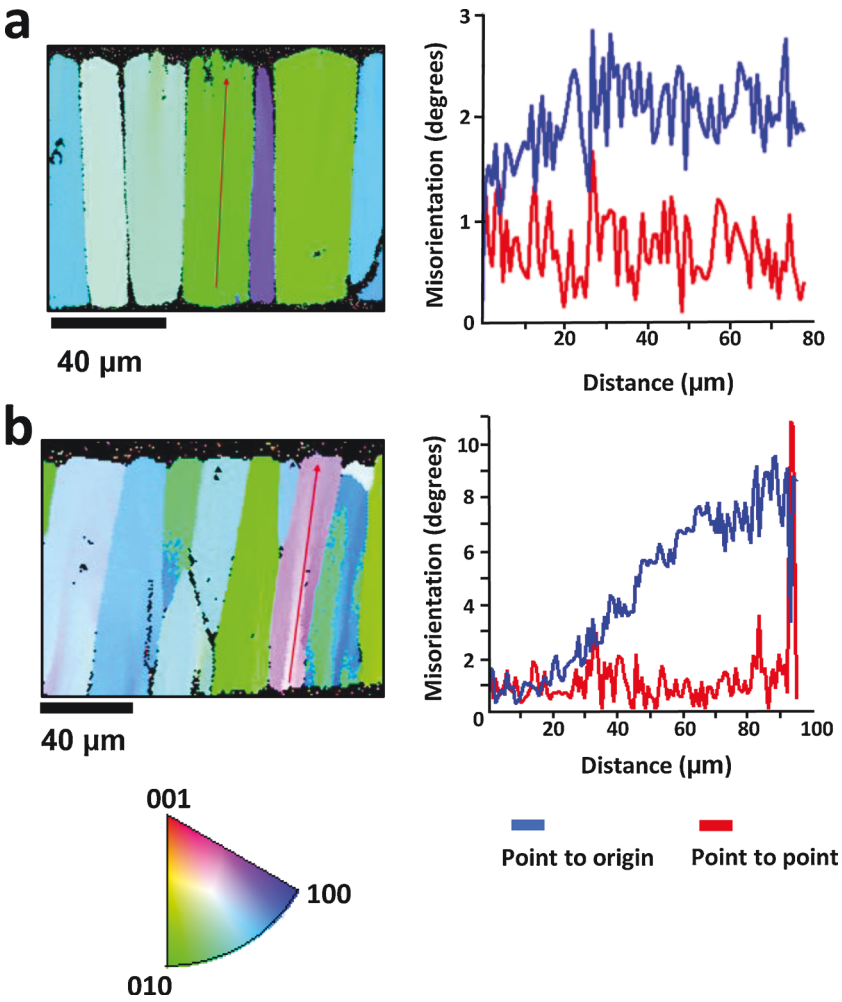

Fig. 3. EBSD analysis of prisms. The cross section of prismatic layer was prepared and observed by SEM for EBSD measurements. a, prisms of non-injection; b, prisms of allosamidin injection. The left images show the crystal orientation maps overwrapping the SEM images. Colors denote the crystallographic direction according the lower insert ({001} in red, {010} in green and {100} in blue). Right graphs are line profiles from the origin to the end of arrows described in the maps. Red lines show an absolute value and blue lines show a relative value to the previous point.

pressure (Kim et al., 2016). The crystal distortion blocked transmission of strength to inhibit propagation of a crack. Because allosamidin treatment caused crystal distortions in calcite prisms, we investigated how such crystal distortions influenced mechanical properties such as hardness and the elastic modulus of calcite prisms. To examine the mechanical properties of calcite prisms, nanoindentation analysis of the prism surface was conducted. A nanoindentation force-displacement curve was drawn from the applied load *versus* depth profile, and hardness and the elastic modulus were obtained from this curve. The force-displacement curves are shown in Fig. 4a and b. When a force was loaded up to 100 mN, the maximum displacement was approximately 1–3 μm in the non-injection treatment (measurements at eight points). However, with allosamidin treatment, the maximum displacement was approximately 1–1.5 μm (measurements at six points). In addition, the cracks caused by indentation following allosamidin treatment were blocked to a greater extent than the non-injection treatment (Fig. S6), and both hardness and the reduced elastic modulus of prisms following allosamidin treatment increased by approximately 80.6 % and 105 %, respectively, compared with those of the non-injection treatment (Fig. 4c). These results indicated that inhibition of chitinase activity strengthened prisms, likely because crystal defects observed by EBSD could prevent the motion of dislocation in a crystal. Crystals contain a few dislocations that exist along the end of an extra half-plane of atoms (Callister and Rethwisch, 2009). Because the force field around dislocation creates a strain, a dislocation easily moves along the plane perpendicular to the end of an extra half-plane when a shear stress is applied. The dislocation motion causes a slip of the crystal plane. Thus, reducing the dislocation motion results in enhanced mechanical strength. A grain boundary caused by a misorientation or enclosing substance is one factor that can reduce the dislocation motion. This theory could enable us to examine why a biotic calcite containing slight crystal distortions was stronger than abiotic calcite. In the present study, because micro-EBSD mapping revealed crystal misorientation in prisms treated with an inhibitor, this crystal defect may have resulted in harder prisms than normal.

4. Conclusion

This study investigated the effect of chitinolytic enzymes for the formation of calcite crystals in *vivo* and *vitro*. We identified chitin and chitinolytic enzymes as the components of intra-organic matrices included in the calcification of prisms in the prismatic layer of *P. fucata*. Although previous studies have reported that the genes of chitinolytic enzymes were expressed in some species of bivalves, there were no clear evidences that chitinolytic enzymes were associated with calcification. TEM observations and APT measurements showed that the degraded chitin nanofibers were included inside the calcium carbonate. The treatments using the inhibitor of chitinase (allosamidin) for living *P. fucata* affected the misorientation of prisms and changed the toughness and stiffness of the prisms. These results probably lead to develop a new method to produce the strong materials. Our researches in this report could therefore provide new possibilities for further development of biomineralization and material engineering.

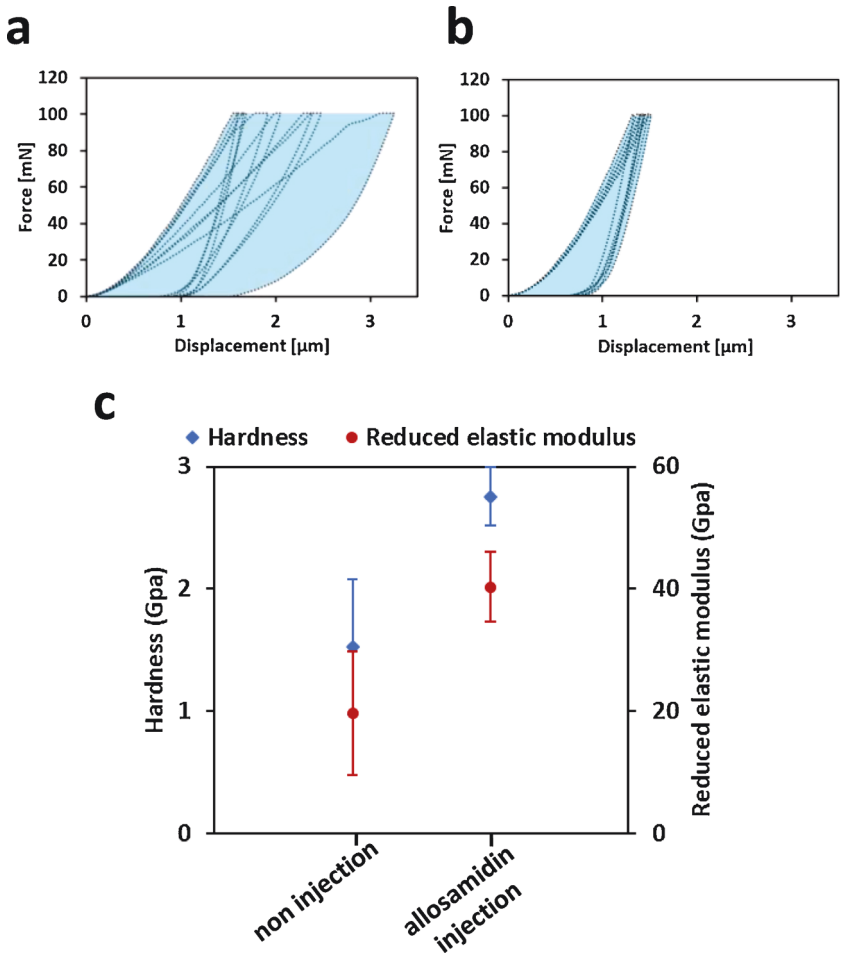

Fig. 4. Measurement of mechanical properties on prisms using nanoindentation. a, b, force-displacement curves measured using nanoindentation; a, in non-injection prism measured at eight points; b, in allosamidin injection prisms measured at six points. A force was loaded up to 100 mN, followed by unloading. Blue shade denotes the spread of displacement. c, hardness and reduced elastic modulus calculated from nanoindentation data.

Availability of data and materials

All data in this study are included in this published article and its supplementary file.

Declaration of Competing Interest

The authors declare that they have no competing interests.

Acknowledgements

This research was partially funded by an Israel Science Foundation (ISF) – Japan Society for the Promotion of Science (JSPS) Joint Academic Research Program, Grant-in-Aid for Young Scientists B (JP16K20995), Grant-in-Aid for Scientific Research B (JP19H03045), Grant-in-Aid for Scientific Research on Innovative Areas IBmS: JSPS KAKENHI Grant Number JP19H05771 to MS, Grant-in-Aid for JSPS Fellows (DC2) to HK. A. P-H. acknowledges support for the APT work from the U.S. National Science Foundation (NSF), grant number EAR-1647012. We would like to thank Shohei Sakuda at Department of Biosciences, Faculty of Science and Engineering, Teikyo University for providing allosamidin and Naoshi Kakio at Shimadzu corporation for helping the nanoindentation analysis.

Appendix A. Supplementary data

Supplementary material related to this article can be found, in the online version, at doi:https://doi.org/10.1016/j.micron.2021.103063.

References

Callister, W.D., Rethwisch, D.G., 2009. Materials Science and Engineering: an Introduction (eighth Edition), eighth edi. John Wiley & Sons Inc.

Checa, A.G., Rodríguez-Navarro, A.B., Esteban-Delgado, F.J., 2005. The nature and formation of calcitic columnar prismatic shell layers in pteriomorphian bivalves. Biomaterials 26, 6404–6414. https://doi.org/10.1016/j.biomaterials.2005.04.016.

Dauphin, Y., Zolotoyabko, E., Berner, A., Lakin, E., Rollion-Bard, C., Cuif, J.P., Fratzl, P., 2019. Breaking the long-standing morphological paradigm: individual prisms in the pearl oyster shell grow perpendicular to the c-axis of calcite. J. Struct. Biol. 205, 121–132. https://doi.org/10.1016/j.jsb.2019.01.004.

Furuhashi, T., Beran, A., Blazso, M., Czegeny, Z., Schwarzinger, C., Steiner, G., 2009a. Pyrolysis GC/MS and IR spectroscopy in chitin analysis of molluscan shells. Biosci. Biotechnol. Biochem. 73, 93–103. https://doi.org/10.1271/bbb.80498.

Furuhashi, T., Schwarzinger, C., Miksik, I., Smrz, M., Beran, A., 2009b. Molluscan shell evolution with review of shell calcification hypothesis. Comp. Biochem. Physiol. - B Biochem. Mol. Biol. 154, 351–371. https://doi.org/10.1016/j.cbpb.2009.07.011.

Gao, H., Ji, B., Jäger, I.L., Arzt, E., Fratzl, P., 2003. Materials become insensitive to flaws at nanoscale: lessons from nature. Proc. Natl. Acad. Sci. U. S. A. 100, 5597–5600. https://doi.org/10.1073/pnas.0631609100.

Gilbert, P.U.P.A., Abrecht, M., Frazer, B.H., 2005. The organic-mineral interface in biominerals, in: molecular Geomicrobiology. Rev. Mineral. Geochem. 59, 157–185. https://doi.org/10.2138/rmg.2005.59.7.

Gilbert, P.U.P.A., Young, A., Coppersmith, S.N., 2011. Measurement of c-axis angular orientation in calcite (CaCO3) nanocrystals using X-ray absorption spectroscopy. Proc. Natl. Acad. Sci. U. S. A. 108, 11350–11355. https://doi.org/10.1073/pnas.1107917108.

Gordon, L.M., Tran, L., Joester, D., 2012. Atom probe tomography of apatites and bone-type mineralized tissues. ACS Nano 6, 10667–10675. https://doi.org/10.1021/nn3049957.

Ifuku, S., Nogi, M., Yoshioka, M., Morimoto, M., Yano, H., Saimoto, H., 2010. Fibrillation of dried chitin into 10-20 nm nanofibers by a simple grinding method under acidic

conditions. Carbohydr. Polym. 81, 134–139. https://doi.org/10.1016/j.carbpol.2010.02.006.
Jackson, A.P., Vincent, J.F.V., Turner, R.M., 1988. The mechanical design of nacre. Proc. R. Soc. London. Ser. B. Biol. Sci. 234, 415–440. https://doi.org/10.1098/rspb.1988.0056.
Kamat, S., Su, X., Ballarini, R., Heuer, A.H., 2000. Structural basis for the fracture toughness of the shell of the conch <i>Strombus gigas<i/>. Nature 405, 1036–1040. https://doi.org/10.1038/35016535.
Kim, Y.-Y., Carloni, J.D., Demarchi, B., Sparks, D., Reid, D.G., Kunitake, M.E., Tang, C.C., Duer, M.J., Freeman, C.L., Pokroy, B., Penkman, K., Harding, J.H., Estroff, L.A., Baker, S.P., Meldrum, F.C., 2016. Tuning hardness in calcite by incorporation of amino acids. Nat. Mater. 15, 903–910. https://doi.org/10.1038/nmat4631.
Kintsu, H., Okumura, T., Negishi, L., Ifuku, S., Kogure, T., Sakuda, S., Suzuki, M., 2017. Crystal defects induced by chitin and chitinolytic enzymes in the prismatic layer of *Pinctada fucata*. Biochem. Biophys. Res. Commun. 489, 89–95. https://doi.org/10.1016/J.BBRC.2017.05.088.
Levi-Kalisman, Y., Falini, G., Addadi, L., Weiner, S., 2001. Structure of the nacreous organic matrix of a bivalve mollusk shell examined in the hydrated state using Cryo-TEM. J. Struct. Biol. 135, 8–17. https://doi.org/10.1006/jsbi.2001.4372.
Marie, B., Zanella-Cléon, I., Corneillat, M., Becchi, M., Alcaraz, G., Plasseraud, L., Luquet, G., Marin, F., 2011. Nautilin-63, a novel acidic glycoprotein from the shell nacre of *Nautilus macromphalus*. FEBS J. 278, 2117–2130. https://doi.org/10.1111/j.1742-4658.2011.08129.x.
Miyamoto, H., Miyashita, T., Okushima, M., Nakano, S., Morita, T., Matsushiro, A., 1996. A carbonic anhydrase from the nacreous layer in oyster pearls. Proc. Natl. Acad. Sci. U. S. A. 93, 9657–9660. https://doi.org/10.1073/PNAS.93.18.9657.
Montagnani, C., Marie, B., Marin, F., Belliard, C., Riquet, F., Tayalé, A., Zanella-Cléon, I., Fleury, E., Gueguen, Y., Piquemal, D., Cochennec-Laureau, N., 2011. Pmarg-pearlin is a matrix protein involved in nacre framework formation in the Pearl Oyster *Pinctada margaritifera*. Chem. Bio. Chem 12, 2033–2043. https://doi.org/10.1002/cbic.201100216.
Nakahara, H., Bevelander, G., 1971. The formation and growth of the prismatic layer of *Pinctada radiata*. Calcif. Tissue Res. 7, 31–45. https://doi.org/10.1007/BF02062591.
Nudelman, F., Sommerdijk, N.A.J.M., 2012. Biomineralization as an inspiration for materials chemistry. Angew. Chemie Int. Ed. 51, 6582–6596. https://doi.org/10.1002/anie.201106715.
Okumura, T., Suzuki, M., Nagasawa, H., Kogure, T., 2010. Characteristics of biogenic calcite in the prismatic layer of a pearl oyster, *Pinctada fucata*. Micron 41, 821–826. https://doi.org/10.1016/j.micron.2010.05.004.
Okumura, T., Suzuki, M., Nagasawa, H., Kogure, T., 2012. Microstructural variation of biogenic calcite with intracrystalline organic macromolecules. Cryst. Growth Des. 12, 224–230. https://doi.org/10.1021/cg200947c.
Oliver, W.C., Pharr, G.M., 1992. An improved technique for determining hardness and elastic modulus using load and displacement sensing indentation experiments. J. Mater. Res. 7, 1564–1583. https://doi.org/10.1557/JMR.1992.1564.
Olson, I.C., Metzler, R.A., Tamura, N., Kunz, M., Killian, C.E., Gilbert, P.U.P.A., 2013. Crystal lattice tilting in prismatic calcite. J. Struct. Biol. 183, 180–190. https://doi.org/10.1016/j.jsb.2013.06.006.
Pérez-Huerta, A., Laiginhas, F., Reinhard, D.A., Prosa, T.J., Martens, R.L., 2016. Atom probe tomography (APT) of carbonate minerals. Micron 80, 83–89. https://doi.org/10.1016/J.MICRON.2015.10.001.
Pérez-Huerta, A., Suzuki, M., Cappelli, C., Laiginhas, F., Kintsu, H., 2019. Atom probe tomography (APT) characterization of organics occluded in single calcite crystals: implications for biomineralization studies. C — J. Carbon Res. 5, 50. https://doi.org/10.3390/c5030050.
Sakuda, S., Isogai, A., Matsumoto, S., Suzuki, A., 1987. Search for microbial insect growth regulators. II. Allosamidin, a novel insect chitinase inhibitor. J. Antibiot. (Tokyo). 40, 296–300.
Sudo, S., Fujikawa, T., Nagakura, T., Ohkubo, T., Sakaguchi, K., Tanaka, M., Nakashima, K., Takahashi, T., 1997. Structures of mollusc shell framework proteins. Nature 387, 563–564. https://doi.org/10.1038/42391.
Suzuki, M., Sakuda, S., Nagasawa, H., 2007. Identification of chitin in the prismatic layer of the shell and a chitin synthase gene from the Japanese pearl oyster, *Pinctada fucata*. Biosci. Biotechnol. Biochem. 71, 1735–1744. https://doi.org/10.1271/bbb.70140.
Suzuki, M., Saruwatari, K., Kogure, T., Yamamoto, Y., Nishimura, T., Kato, T., Nagasawa, H., 2009. An acidic matrix protein, Pif, is a key macromolecule for nacre formation. Science 325, 1388–1390. https://doi.org/10.1126/science.1173793.
Suzuki, M., Iwashima, A., Tsutsui, N., Ohira, T., Kogure, T., Nagasawa, H., 2011. Identification and characterisation of a calcium carbonate-binding protein, blue mussel shell protein (BMSP), from the nacreous layer. ChemBioChem 12, 2478–2487. https://doi.org/10.1002/cbic.201100317.
Suzuki, M., Nakayama, S., Nagasawa, H., Kogure, T., 2013. Initial formation of calcite crystals in the thin prismatic layer with the periostracum of *Pinctada fucata*. Micron 45, 136–139. https://doi.org/10.1016/J.MICRON.2012.10.010.
Tamura, H., Nagahama, H., Tokura, S., 2006. Preparation of chitin hydrogel under mild conditions. Cellulose 13, 357–364. https://doi.org/10.1007/s10570-006-9058-z.
Valley, J.W., Cavosie, A.J., Ushikubo, T., Reinhard, D.A., Lawrence, D.F., Larson, D.J., Clifton, P.H., Kelly, T.F., Wilde, S.A., Moser, D.E., Spicuzza, M.J., 2014. Hadean age for a post-magma-ocean zircon confirmed by atom-probe tomography. Nat. Geosci. 7, 219–223. https://doi.org/10.1038/ngeo2075.
Weiner, S., Hood, L., 1975. Soluble protein of the organic matrix of mollusk shells: a potential template for shell formation. Science 190, 987–989.
Weiner, S., Traub, W., 1980. X-ray diffraction study of the insoluble organic matrix of mollusk shells. FEBS Lett. 111, 311–316. https://doi.org/10.1016/0014-5793(80)80817-9.
Weiner, S., Traub, W., Parker, S.B., 1984. Macromolecules in mollusc shells and their functions in biomineralization. Philos. Trans. R. Soc. London. B, Biol. Sci. 304, 425–434. https://doi.org/10.1098/rstb.1984.0036.